ISSN 0031-918X, Physics of Metals and Metallography, 2022, Vol. 123, No. 10, pp. 1041–1047. © Pleiades Publishing, Ltd., 2022.
Russian Text © The Author(s), 2022, published in Fizika Metallov i Metallovedenie, 2022, Vol. 123, No. 10, pp. 1109–1116.

STRENGTH AND PLASTICITY

The Effect of Prolonged Annealing on the Structural Stability of Nanoparticle-Hardened Low-Carbon 9% Cr–3% Co Steel

A. E. Fedoseeva[a], * and S. I. Degtyareva[a]

[a] *Belgorod State University, Belgorod, 308015 Russia*

**e-mail: fedoseeva@bsu.edu.ru*

Received June 24, 2022; revised July 26, 2022; accepted August 5, 2022

Abstract—The effect of long-term annealing on the structure of low-carbon 9% Cr–3% Co steel hardened with nanoparticles has been studied. Annealing was performed for 100, 500, 1000, and 3000 hours at a temperature of 650°C. After heat treatment, the width of martensitic laths in the steel structure was about 300 nm and the dislocation number density inside the laths was high. The lath structure of tempered martensite was stabilized by (Ta,Cr)X carbonitrides with an average size of 11 nm. The Vickers microhardness decreased by 16% after 3000-h annealing compared to that of the initial state. The decrease in microhardness was accompanied by structural changes in the steel upon annealing, such as a decrease in the dislocation density, a decrease in the content of tungsten and copper in the solid solution, and the enlargement of carbonitrides (Ta,Cr)X and martensitic laths. In general, the structural stability of the investigated steel during long-term annealing is quite high compared to that of other high-chromium martensitic steels.

Keywords: martensitic high-temperature steel, heat treatment, prolonged annealing, microstructure, secondary phase particles, softening

DOI: 10.1134/S0031918X22600889

INTRODUCTION

The development of coal-fired thermal power plants aims to increase efficiency using ultrasupercritical steam parameters [1–3]. High-chromium martensitic steels are promising materials for manufacturing elements of pipes, boilers, blades, and rotors of new power units [3]. The structure of these steels is a lath tempering martensite stabilized by various types of secondary phase particles [4]. MX carbonitrides (where M is vanadium, niobium, tantalum, and their combination; X is carbon, nitrogen, and their combination) with sizes from 5 to 50 nm show the most effective hardening, They precipitate uniformly over the matrix volume during the normalizing of steel (usually these are niobium, and/or tantalum carbides) and its tempering (vanadium, niobium, and/or tantalum nitrides) [4–6] and serve as barriers to the movement of free dislocations and their rearrangement into low-energy configurations [5, 6]. However, these particles are nonequilibrium and they transform into large Z-phase particles in the process of operation at 600–650°C [6]. A new model chemical composition of 9% Cr steel with a low carbon content and high nitrogen and tantalum content was developed to provide for precipitation of fine *Z*-phase particles in the initial state during thermomechanical treatment [7, 8]. However, the standard heat treatment results in the precipitation of nonequilibrium MX-carbonitride dispersion [7]. The short-term tensile properties after the standard heat treatment, which caused the formation of MX carbonitrides, and thermomechanical treatment, which led to the precipitation of *Z*-phase particles, were similar, which was explained by the close sizes and volume fractions of MX carbonitrides and *Z*-phase particles [7]. This work aimed to test the thermal stability of the structure in a new model steel hardened with nonequilibrium MX nanoparticles precipitated during standard heat treatment and to find the relationship between the structural changes and the hardness of the material. The next series of works will be aimed at testing the stability of the structure hardened by equilibrium *Z*-phase nanoparticles.

EXPERIMENTAL

Low-carbon 9% Cr steel with a chemical composition (wt %) of 0.02% C–8.2% Cr–1.84% W–2.83% Co–2.16% Cu–0.34% Ta–0.21% Si–0.14% Mn–0.08% Ni–0.016% N–0.009% Al was melted in a vacuum induction furnace. Heat treatment of the steel included quenching from 1200°C at a holding time of 16 h, cooling in air, and subsequent tempering at 750°C for 3 hours followed by air cooling. This was the initial state. Prolonged annealing was carried out in an electric resistance furnace at 650°C for 100, 500, 1000, and 3000 h. Vickers microhardness was measured using an AFFRI DM-8 automatic micro-

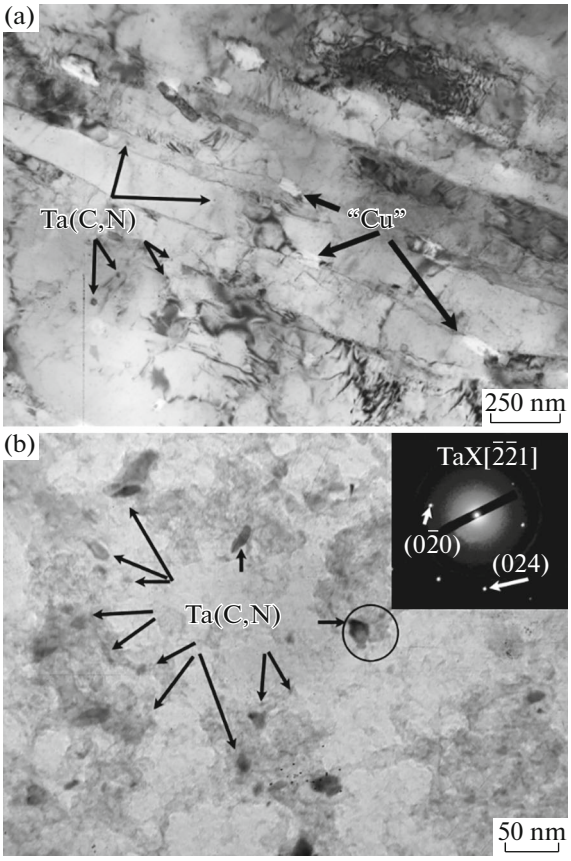

Fig. 1. TEM images of the steel microstructure after quenching at 1200°C and tempering at 750°C: (a) foils and (b) carbon replicas.

hardness tester at a load of 0.3 kg. Structural examinations were performed using a Jeol JEM-2100 transmission electron microscope (TEM) equipped with an energy dispersive spectrometry (INCA) attachment and a Quanta 600 scanning electron microscope (SEM) equipped with an EDX attachment. The foils for TEM and SEM examinations were mechanically thinned to 0.15 mm and then electrolytically polished in an electrolyte of 10% perchloric acid in acetic acid. Carbon replicas for the TEM examination were prepared by electrolytic stripping of the carbon film from the sample surface in 10% hydrochloric acid in ethyl alcohol electrolyte at 15 V for 2 s. The size of martensitic laths was estimated by the random linear intercept method using at least six TEM images. The dislocation number density was calculated as the number of points where dislocations exit on the upper and lower surfaces of a foil, and at least six TEM images were analyzed. Secondary-phase particles were identified from carbon replicates by analyzing the local chemical composition and electron diffraction patterns. At least 300 particles were analyzed for each state. The phase composition and the volume fractions of the secondary-phase particles were calculated by computer simulation using Thermo-Calc software. The growth kinetics of secondary-phase particles were estimated by computer simulation using Thermo-Calc and Prisma software, with data extrapolated to 100000 hours.

RESULTS AND DISCUSSION

The Steel Structure after Heat Treatment

Figure 1 shows TEM images of the structure after heat treatment. Heat treatment results in the formation of a tempered martensite structure with an average martensite lath cross-section size of about 300 ± 30 nm and a high dislocation number density of 4.6×10^{14} m^{-2}. The structure exhibited secondary phase particles, such as MX carbonitrides uniformly distributed over the matrix volume, large Laves phases (Fe_2W), Cu-enriched particles located at the boundaries of the initial austenitic grains, and martensitic laths. The average size of the Cu-enriched particles was 55 ± 5 nm, but their fraction was insignificant. The MX carbonitrides were enriched with tantalum to have a chemical composition of 86.0% Ta–13.8% Cr–0.2% Fe.

The average size of these particles was 11 ± 2 nm. There were also MX carbonitrides additionally enriched with tantalum and titanium to the following chemical composition: 78.4% Ta–11% Cr–10% Ti–0.6% Fe. The average size of these particles was 49 ± 5 nm. The (Ta,Cr,Ti)X particles probably remained insoluble during the quenching process, while fine (Ta,Cr)X particles precipitated upon subsequent tempering. The volume fraction of all TaX carbonitrides was 0.19%, and the fraction of large (Ta,Cr,Ti)X particles did not exceed 10% of all TaX. The ferritic matrix was enriched with 8.2 ± 0.1 wt % chromium, 1.8 ± 0.1 wt % tungsten, and 2.0 ± 0.1% copper. This structure has a rather high Vickers microhardness of 256 ± 5 $HV_{0.3}$.

Hardness Behavior upon Prolonged Annealing at 650°C

Table 1 presents data on the effect of long annealing time on Vickers hardness. In addition, there are data for two other high-chromium steels of the following chemical compositions (wt %): 0.1% C–0.03% N–10% Cr–1.4% Mn–1.4% Co–1.4% W–0.34% (V + Nb + Ta) and 0.001% C–0.042% N–9.5% Cr–1.2% Mn–1.5% Co–1.4% W–0.34% (V + Nb + Ta) [9]. The behavior of the hardness decrease of the 0.1C–0.03N–10Cr steel is very similar to that of the studied steel, despite the fact that the steel with 0.1% carbon content additionally has a stable hardening phase such as grain boundary carbide $M_{23}C_6$ [9, 10]. In contrast, the 0.001C–0.04N–9.5Cr steel, whose composition is close to that of the studied steel, shows a significant decrease in microhardness during prolonged annealing (Table 1). The difference in microhardness of the studied steel and the 0.001C–0.04N–9.5Cr steel was 33% after prolonged 3000-h annealing

Table 1. Data on the effect of the annealing time on the Vickers hardness $HV_{0.3}$ of the investigated steel in the units of $HV_{0.3}$ in comparison with other steels [9]

Annealing time, h	Steel	0.1% C–0.03% N–10%Cr	0.001% C–0.04% N–9.5%Cr
0	256 ± 5	239	214
100	256 ± 10	235	197
500	247 ± 5	230	191
1000	227 ± 5	222	183
3000	217 ± 5	216	136

(Table 1). Similar softening of 0.001C–0.04N–9.5Cr steel was explained by the significant enlargement of MX carbonitrides during annealing [9]. The stability of (Ta,Cr)X carbonitrides is the key to the structural stability during annealing.

The Evolution of the Steel Structure after Prolonged Annealing

Figures 2 and 3 show images of the microstructure and secondary phase particles after prolonged annealing at different holding times. The lath structure of tempered martensite is retained even after 3000-h annealing (Fig. 2d). The width of martensitic laths remains constant (about 300 ± 30 nm) up to 1000 h of annealing and increases to 370 ± 30 nm after 3000-h annealing. The dislocation number density continuously decreases with increasing annealing time. A significant decrease in the dislocation number density by a factor of two was found after 500 h compared to that after the initial heat treatment. After 3000 h, the dislocation number density was $(1.4 \pm 0.5) \times 10^{14}$ m^{-2}. The chemical composition of the ferritic matrix and the phase composition of the investigated steel changed during the prolonged annealing. First, the reduction of tungsten content in the solid solution to 1.0 ± 0.1 wt % after 1000 h was accompanied by the precipitation of a large number of Laves phase particles, mainly at boundaries of initial austenitic grains, packets, and blocks (Figs. 2a, 2c) and their subsequent significant

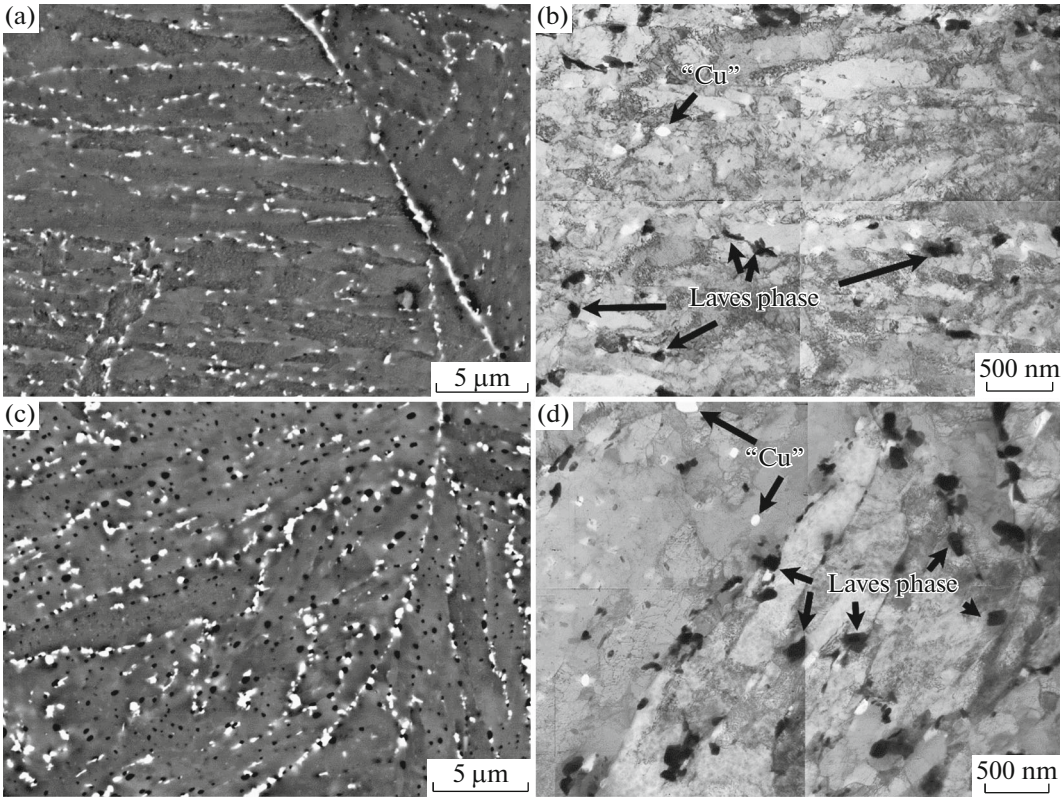

Fig. 2. (a), (c) SEM and (b), (d) TEM images of the steel microstructure after a prolonged annealing at 650°C for (a), (b) 500, and (c), (d) 3000 hours.

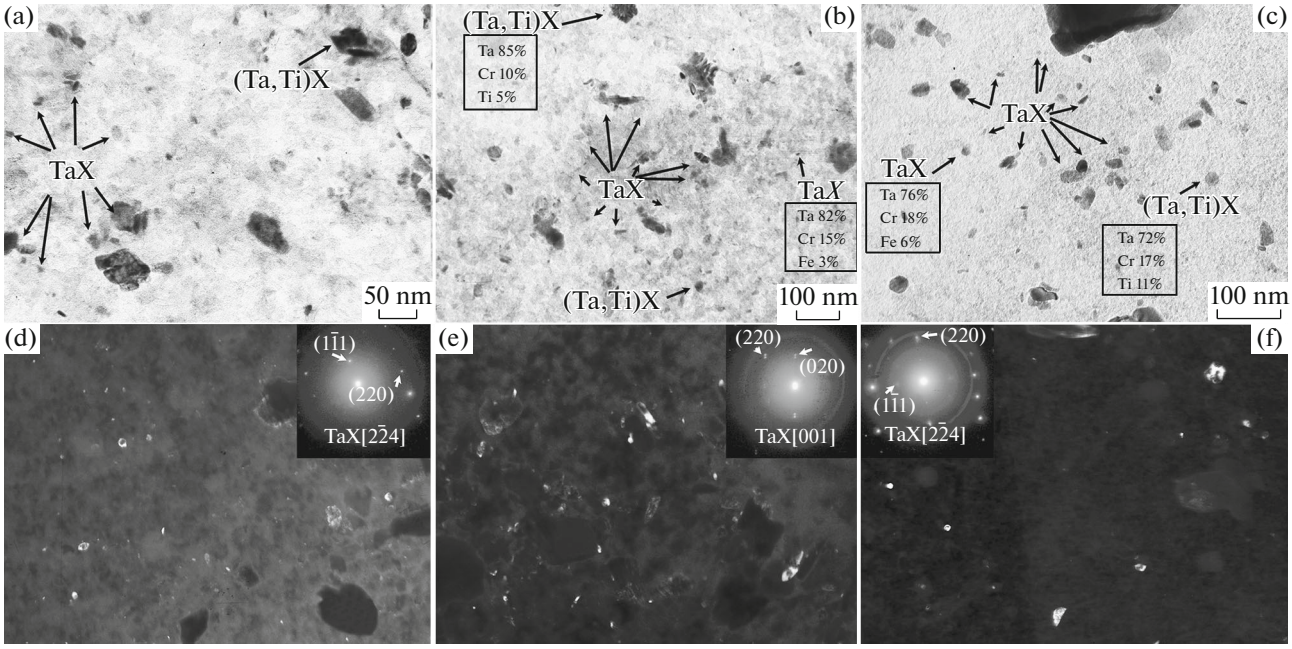

Fig. 3. The TEM images of secondary phase particles in the investigated steel after prolonged annealing at 650°C for (a), (d) 500, (b), (e) 1000, and (c), (f) 3000 hours. (d), (e), (f) Dark-field images taken in (220)[2$\bar{2}$4], (220)[001], and (220)[2$\bar{2}$4] reflections of TaX carbonitride, respectively (d–f).

growth. The Laves phase particles were detected at boundaries of martensitic laths (Figs. 2b, 2d). The average size of these particles exceeded 100 nm, even after 500-h annealing, which indicates that the particles of this phase do not make a contribution to the hardening from the lath structure. Second, the copper content in the solid solution decreased together with the formation of Cu-enriched particles at boundaries of martensitic laths (Figs. 2b, 2d). The average size of Cu-enriched particles increased from 55 ± 6 nm after 100-h annealing to 149 ± 10 nm after 3000-h annealing. The volume fraction of these particles was 2% at 650°C after 500 h. Third, (Ta,Cr)X carbonitrides sharply enlarged from 13 ± 2 nm after 1000-h annealing to 16 ± 2 nm after 3000-h annealing (Figs. 3b–3f). The volume fraction of these particles remained at around 0.19%. The enlargement of (Ta,Cr)X particles was accompanied by an increase in the chromium and iron content to 24 wt % and a decrease in the tantalum content to 76 wt % in the chemical composition of this phase (Fig. 3c). We should note that no transformation of nonequilibrium (Ta,Cr)X carbonitride into stable equilibrium *Z*-phase (CrTaN) particles occurred upon prolonged annealing, which has also been found for 9% Cr steel containing 0.1% C [5].

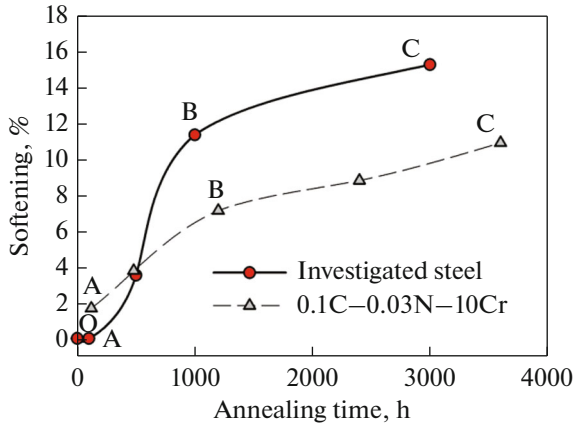

Fig. 4. Softening (%) vs. the annealing time. For comparison, here are data for 0.1C–0.03N–10Cr steel [9].

The Microstructural Aspects of Steel Cracking during Prolonged Annealing

Prolonged annealing develops static recovery in steel, which manifests itself in the annihilation of dislocations, enlargement of particles, and enlargement of martensitic laths, leading to the softening of the material. Softening of the studied steel can be expressed through the following parameter [9]:

$$\mu = 1 - HV_{\text{anneal}}/HV_0, \quad (1)$$

where μ is the softening parameter, HV_{anneal} is the Vickers microhardness after annealing, and HV_0 is the Vickers microhardness after the initial heat treatment (both HV are in the units $HV_{0.3}$). Figure 4 shows the dependence of softening on the annealing time.

The softening curve for the investigated steel can be divided into three sections. The first OA region corresponds to the first 100 h of annealing; there is no softening in it. This agrees well with the data that there are no significant structural changes in the steel during this short annealing period. The second AB region, corresponding to the annealing time from 100 to 1000 h, is characterized by a sharp softening by almost 12%. This softening is caused by two factors simultaneously: a decrease in the tungsten content in the solid solution to the equilibrium content and a decrease in the dislocation number density. The decrease in the free dislocation number density by 50% is due to the annihilation of dislocations of different signs. This process prevails in the first 500 h. Subsequent annealing decreases the dislocation number density only by a factor of 1.3. The escape of tungsten from the solid solution proceeds most actively in the range from 500 to 1000 h of annealing, which facilitates dislocation motion, annihilation, and rearrangement into low-energy dislocation structures: cells, networks, dislocation boundaries, and low-angle boundaries. There is no visible growth of martensitic laths in this region due in part to a relative balance between the growth of "existing" laths due to the migration of triple junctions and the formation of "new" boundaries due to the rearrangement of dislocations into low-angle boundaries. The third BC region, corresponding to the annealing time from 1000 to 3000 h, is characterized by a smooth decrease in softening. The softening in this region is caused by the enlargement of (Ta,Cr)X particles and the enlargement of martensitic laths. We should note that no "new" boundaries form in this case and the number density of free dislocations does not change.

The relationship between particle size and martensitic lath size can be expressed through the balance between the driving and retarding forces of recrystallization and can be described as [11]:

$$d_{\text{laths}} = 2d_{\text{particle}}/3\alpha Fv, \qquad (2)$$

where d_{lathes} is the equilibrium size of the laths, d_{particle} is the average size of (Ta,Cr)X carbonitrides, Fv is the volume fraction of (Ta,Cr)X carbonitrides at 650°C (0.185%), α is the proportionality coefficient, equal to 13 [11]. The size of the laths during annealing depends, therefore, on the particle size and the particle volume fraction. To predict the lath size after 100000-h annealing, the kinetics of particle growth was simulated using Thermo-Calc and Prisma software. The results are shown in Fig. 5.

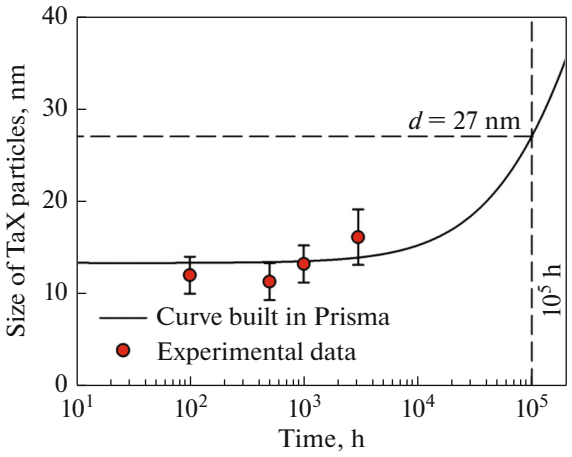

Fig. 5. Simulation of (Ta,Cr)X particle growth based on experimental data.

Simulation of (Ta,Cr)X particle growth using experimental data showed that the particle size after 100000-h annealing at 650°C is 27 nm, assuming that the volume fraction of 0.185% is retained. Analysis of the balance between the driving and retarding forces of recrystallization, as presented in Table 2, revealed good agreement between the lath sizes calculated by Eq. (2) and the experimental data. The maximum difference in the values was about 20% (Table 2). This indicates that (Ta,Cr)X particles are responsible for the enlargement of martensitic laths upon a prolonged annealing process. For example, 100000-h annealing results in the size of martensitic laths of 750 nm when the average ((Ta,Cr)X) particle size is 27 nm. According to Fig. 4, this enlargement of particles and martensitic laths does not cause significant softening of the material.

For comparison, Fig. 4 presents data on the softening of 0.1C–0.03N–10Cr steel [9]. The character of

Table 2. The experimental data on the sizes of (Ta,Cr)X particles and martensitic laths in comparison with the equilibrium sizes of laths calculated by Eq. (2)

Annealing conditions, h	Size of (Ta,Cr)X particles, nm	Experimental laths size, nm	Calculated lath size, nm
0	11 ± 2	290 ± 30	290
100	12 ± 2	300 ± 30	330
500	11 ± 2	300 ± 30	320
1000	13 ± 2	300 ± 30	370
3000	16 ± 2	370 ± 30	450
100000	27	–	750

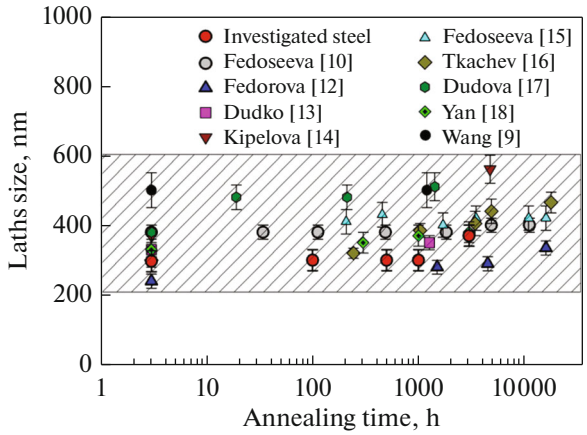

Fig. 6. The size of martensitic laths upon prolonged annealing in the investigated steel in comparison with that in other high-chromium steels [9, 10, 12–18].

the softening of the 0.1C–0.03N–10Cr steel is similar to that of the studied steel. There are also three stages of softening, which are supposedly caused by the same factors described above for the investigated steel, although they were not described in [9]. The lower degree of softening at the AB region is caused by the lower content of tungsten in 0.1C–0.03N–10Cr steel (1.4 wt %) and, accordingly, the smaller difference between the excess of tungsten content and its equilibrium value. The slopes of the BC region for the 0.1C–0.03N–10Cr steel and the studied steel are the same, which indicates that martensitic laths grow at the same rate in both steels.

Therefore, softening processes in high-chromium steels upon annealing are universal (provided that there are no recrystallization processes) regardless of steel alloying.

A Comparison of the Structural Stabilities during Prolonged Annealing for the Steel under Study and other Steels

The stability of the size of martensitic laths indicates the structural stability of high-chromium steels during prolonged annealing or creep. To estimate the structural stability during prolonged annealing, the martensitic lath size dynamics were analyzed comparing the studied steel with other martensitic steels. The comparative analysis is shown in Fig. 6. The compared steels contained 9–10% Cr–(0–3)% Co–(1–3)% W–(0–1)% Mo–(0–0.2)% V–(0–0.05)% Nb–(0–0.1)% Ta, but differed significantly in carbon, nitrogen, and boron contents [9, 10, 12–19]. Figure 6 shows that the scattering of the lath size values during prolonged annealing at 650°C for 30 000 h is in the range from 200 to 600 nm. The lath sizes in the studied steel correspond to the above range, and even belong to its lower part. We note that many steels, even those with stable secondary phases, experience growth of martensitic laths after a 1000-h annealing, but the lath width does not exceed 600 nm. The stability of the structure in the investigated low-carbon 9% Cr steel hardened with nonequilibrium particles during prolonged annealing is high and corresponds to the stability level of other high-chromium steels.

CONCLUSIONS

The effects of prolonged annealing at 650°C for 100, 500, 1000, and 3000 h on the structural stability of low-carbon 9% Cr–3% Co steel were revealed The steel structure after the initial heat treatment was a tempered martensite with an average size of about 300 nm and a high dislocation number density. The structure was stabilized by (Ta,Cr)X particles with an average size of 11 nm. The microhardness of this structure was 256 $HV_{0.3}$.

Prolonged annealing resulted in the softening of the material. The softening was expressed through the ratio between the post-annealing microhardness and the initial microhardness. During prolonged annealing, the main structural changes leading to softening are dislocation annihilation and a decrease in tungsten content in the solid solution during the first 1000 h of annealing, and enlargement of (Ta,Cr)X particles together with enlargement of martensitic laths in the annealing time range of 1000 to 3000 h. The stability of the structure in the low-carbon 9% Cr steel during annealing is high and corresponds to the stability level of other high-chromium steels.

ACKNOWLEDGMENTS

We thank the Technologies and Materials Center for Collective Use at Belgorod State University, which is financially supported by the Ministry of Science and Higher Education of the Russian Federation under Agreement no. 075-15-2021-690.

FUNDING

This work was carried out within the framework of Russian Federation President's grant for state support of young Russian scientists-candidates of sciences (grant no. MK-1995.2021.4).

CONFLICT OF INTEREST

The authors declare that they have no conflicts of interest.

REFERENCES

1. R. Kaibyshev, V. Skorobogatykh, and I. Shchenkova, "New martensitic steels for fossil power plant: Creep resistance," Phys. Met. Metallogr. **109**, 186–200 (2010).
2. V. Skorobogatykh and I. Shchenkova, "Development and mastering of materials for thermal blocks for super-

supercritical parameters," Energonadzor i Energobezopasnost' **1**, 56–59 (2008).

3. F. Abe, T. U. Kern, and R. Viswanathan, *Creep-Resistant Steels* (Woodhead, Cambridge, 2008).
4. A. E. Fedoseeva, I. S. Nikitin, and R. O. Kaibyshev, "Effect of the quenching temperature on the creep resistance of 9% Cr–1% W–1% Mo–V–Nb martensite steel," Phys. Met. Metallogr. **123** (1), 92–98 (2022).
5. H. K. Danielsen, "Review of *Z* phase precipitation in 9–12 wt % Cr steels," Mater. Sci. Technol. **32**, 126–137 (2016).
6. A. Fedoseeva, I. Nikitin, N. Dudova, and R. Kaibyshev, "The effect of creep and long annealing conditions on the formation of the *Z*-phase particles," Phys. Met. Metallogr. **121**, 561–567 (2020).
7. A. Fedoseeva, A. Dolzhenko, and A. Fedoseev, "Effect of thermo-mechanical treatment on short-term mechanical properties of low-carbon 9% Cr martensitic steel," AIP Conf. Proc. **2509**, 020072 (2022).
8. A. Fedoseeva and A. Fedoseev, "Modeling of thermomechanical treatment for formation of stable particles in a low-carbon 9% Cr martensitic steel," AIP Conf. Proc. **2509**, 020071 (2022).
9. H. Wang, W. Yan, S. Zwaag, Q. Shi, W. Wang, K. Yang, and Y. Shan, "On the 650°C thermostability of 9–12Cr heat resistant steels containing different precipitates," Acta Mater. **134**, 143–154 (2017).
10. A. Fedoseeva, N. Dudova, and R. Kaibyshev, "Creep strength breakdown and microstructure evolution in a 3% Co modified P92 steel," Mater. Sci. Eng., A **654**, 1–12 (2016).
11. F. J. Humphreys and M. Hatherly, *Recrystallization and Related Annealing Phenomena*, 2nd ed. (Elsevier, Oxford, 2004).
12. I. Fedorova, Zh. Yanushkevich, A. Belyakov, and R. Kaibyshev, "Microstructure and deformation behavior of a hot forged 9% Cr creep resistant steel," Adv. Mater. Res. **409**, 672–677 (2012).
13. V. A. Dudko, A. N. Belyakov, V. N. Skorobogatykh, I. A. Shchenkova, and R. O. Kaibyshev, "Structural changes in refractory steel 10Kh9V2MFBR due to creep at 650°C," Met. Sci. Heat Treat. **52**, 111–117 (2010).
14. A. Yu. Kipelova, A. N. Belyakov, V. N. Skorobogatykh, I. A. Shchenkova, and R. O. Kaibyshev, "Structural changes in steel 10Kh9K3V1M1FBR due to creep," Met. Sci. Heat Treat. **52**, 118–127 (2010).
15. A. Fedoseeva, N. Dudova, and R. Kaibyshev, "Creep behavior and microstructure of a 9Cr–3Co–3W martensitic steel," J. Mater. Sci. **52**, 2974–2988 (2017).
16. E. Tkachev, A. Belyakov, and R. Kaibyshev, "Creep strength breakdown and microstructure in a 9%Cr steel with high B and low N contents," Mater. Sci. Eng., A **772**, 138821 (2020).
17. N. Dudova, R. Mishnev, and R. Kaibyshev, "Creep behavior of a 10% Cr heat-resistant martensitic steel with low nitrogen and high boron contents at 650°C," Mater. Sci. Eng., A **766**, 138353 (2019).
18. P. Yan, Zh. Liu, H. Bao, Y. Weng, and W. Liu, "Effect of microstructural evolution on high-temperature strength of 9Cr–3W–3Co martensitic heat resistant steel under different aging conditions," Mater. Sci. Eng., A **588**, 22–28 (2013).
19. N. S. Nikolaeva, M. V. Leont'eva-Smirnova, and E. M. Mozhanov, "Effect of thermal aging for up to 22 thousand hours on the structural and phase state of ferritic–martensitic steels EK181 and ChS139," Phys. Met. Metallogr. **123**, 489–499 (2022).

Translated by T. Gapontseva